Elsevier Editorial System(tm) for Energy
Manuscript Draft

Manuscript Number: EGY-D-15-00398R1

Title: CFD simulation to investigate heat and mass transfer processes in a membrane-based absorber for water/LiBr absorption cooling systems

Article Type: Full Length Article

Keywords: Heat and mass transfer, Membrane contactors, Plate-and-frame membrane absorber, Absorption refrigeration systems, CFD simulation

Corresponding Author: Prof. Mahmoud Bourouis, Ph.D.

Corresponding Author's Institution: Rovira i Virgili University

First Author: Faisal Asfand, PhD Student

Order of Authors: Faisal Asfand, PhD Student; Youssef Stiriba, PhD; Mahmoud Bourouis, Ph.D.

Abstract: Absorption cooling systems employing membrane based components provide an interesting opportunity to use the technology for small scale applications. Steady-state heat and mass transfer analyses of a water-lithium bromide membrane based absorber are performed. CFD tool ANSYS/FLUENT 14.0 is used to perform the simulation and investigate the behaviour of the heat and mass transfer mechanisms at local levels in the channels. Results show that the solution film thickness is an important parameter which significantly affects the mass transfer mechanism. It was observed that the absorption rate increased by a factor of 3 when the solution channel thickness was reduced from 2 mm to 0.5 mm. In addition, the absorption mass flux was increased by a factor of 2.5 when the solution inlet flow velocity was increased from 0.00118 m/s to 0.00472 m/s. The solution film thickness and velocity can be independently controlled in plate-and-frame membrane based absorbers. Therefore to design a compact and efficient plate-and-frame membrane absorber with water as a refrigerant, an optimum value of 0.5 mm for the solution film thickness is suggested and a solution velocity of about 0.003 - 0.005 m/s is recommended to achieve high absorption rates with acceptable pressure drop along the solution channel.

CFD simulation to investigate heat and mass transfer processes in a membrane-based absorber for water-LiBr absorption cooling systems

Faisal Asfand, **Youssef Stiriba**, **Mahmoud Bourouis***

Department of Mechanical Engineering – Universitat Rovira i Virgili,

Av. Països Catalans No. 26, 43007 Tarragona, Spain.

*Corresponding author

Email: mahmoud.bourouis@urv.cat ; Phone: +34 977 55 86 13 ; Fax: +34 977 55 96 91

Keywords: Heat and mass transfer, Membrane contactors, Plate-and-frame membrane absorber, Water-lithium bromide, Absorption cooling systems, CFD simulation

Highlights

1) Heat and mass transfer in a water-LiBr membrane based absorber are analysed using CFD approach.
2) Absorption rate increases by a factor of 3 when the solution channel thickness is reduced from 2 mm to 0.5 mm.
3) Pressure drop along the solution channel increases exponentially with decrease in the solution channel thickness.

Abstract

Absorption cooling systems employing membrane based components provide an interesting opportunity to use the technology for small scale applications. Steady-state heat and mass transfer analyses of a water-lithium bromide membrane based absorber are performed. CFD tool ANSYS/FLUENT 14.0 is used to perform the simulation and investigate the behaviour of the heat and mass transfer mechanisms at local levels in the channels. Results show that the solution film thickness is an important parameter which significantly affects the mass transfer mechanism. It was observed that the absorption rate increased by a factor of 3 when the solution channel thickness was reduced from 2 mm to 0.5 mm. In addition, the absorption mass flux was increased by a factor of 2.5 when the solution inlet flow velocity was increased from 0.00118 m/s to 0.00472 m/s. The solution film thickness and velocity can be independently controlled in plate-and-frame membrane based absorbers. Therefore to design a compact and efficient plate-and-frame membrane absorber with water as a refrigerant, an optimum value of 0.5 mm for the solution film thickness is suggested and a solution velocity of about 0.003 – 0.005 m/s is recommended to achieve high absorption rates with acceptable pressure drop along the solution channel.

Nomenclature:

D	mass diffusion coefficient (m^2/s)
d	membrane pore mean diameter (μm)
E	energy (J)
$\vec{F}$	external body force (N)
$\vec{g}$	gravitational force (m/s^2)
h	enthalpy (J/kg)
I	unit tensor
J	mass transfer flux ($kg/m^2.s$)
k	mass transfer coefficient ($kg/m^2.s.Pa$)
M	molecular weight (g/mol)
P	pressure (Pa)
p	static pressure (Pa)
p_{ms}	vapour pressure of solution (Pa)
R	universal gas constant (J/mol.K)
S_h	heat source term ($J/m^3.s$)
S_m	mass source term ($kg/m^3.s$)
T	temperature (^oC, K)

73	Y	mass fraction

74 **Greek letters:**

75	ρ	density (kg/m^3)
76	$\vec{v}$	velocity vector (m/s)
77	ε	porosity
78	δ	thickness (μm)
79	τ	tortuosity
80	λ	thermal conductivity (W/m.K)
81	$\bar{\tau}$	stress tensor
82	μ	dynamic viscosity (kg/m.s)

83 **Subscripts:**

84	*dil*	dilution
85	*eff*	effective
86	i	i^{th} Specie
87	m	membrane
88	p	pore
89	s	solution
90	v	vapour

Chemical Formula:

H_2O water

LiBr lithium bromide

1. Introduction

Absorption refrigeration technology is gaining global acceptance due to its potential for using thermal energy, available from solar thermal energy or waste heat energy sources, instead of mechanical energy. The absorber is an important component of the absorption refrigeration system and plays a critical role in the overall performance, size, and capital cost of the system. Both heat and mass transfer take place simultaneously in the absorber. The design and configuration of the absorber significantly influence its performance. Continued improvements in the design and configuration of the absorber have been suggested by many researchers to improve its performance and thermal efficiency. Both active and passive techniques have been investigated for enhancing the absorption rate in the absorbers of absorption refrigeration systems. These techniques are generally categorized into chemical and mechanical treatments [1, 2]. In mechanical treatments, corrugated surfaces are produced to enhance the heat and mass transfer coefficients. In chemical treatments, the addition of small quantities of additives (surfactants, nanoparticles, etc.) has been extensively investigated. The heat and mass transfer coefficients are enhanced by causing interfacial turbulence. Numerical and experimental research has been performed, using water-LiBr as a working fluid on horizontal and vertical tubes, to investigate the absorption process. Medrano et al. [3] performed an experimental study and achieved an absorption rate of 0.0020 $kg/m^2.s$ for a vertical tube falling film absorber. Jeong and Garimella [4] numerically investigated a horizontal tube falling film absorber and obtained an absorption rate of 0.0023 $kg/m^2.s$. Islam et al. [5] experimentally analysed a horizontal tube falling film absorber with film inversion and achieved an absorption rate of 0.0041 $kg/m^2.s$. Yoon et al. [6] experimentally investigated a helical tube absorber and obtained an absorption rate of 0.0021 $kg/m^2.s$.

131 The use of membrane contactor technology is well-known in the process industry and is
132 growing due to the relative simplicity, reliability, high parameters of separation, large
133 interfacial area and lower energy consumption with improved heat and mass transfer. In
134 recent years, research has been carried out regarding the use of membrane contactors in the
135 form of plate-and-frame membrane modules and hollow fiber membrane modules in
136 absorption refrigeration systems. In the open literature, the plate-and-frame membrane
137 absorber is selected for the absorption refrigeration systems employing water-LiBr as a
138 working fluid mixture, whereas the hollow fiber membrane absorber is selected for the
139 ammonia/water based absorption refrigeration system. The pressure drop in the plate-and-
140 frame membrane module is small; therefore, it is considered a better choice for the water-
141 LiBr working fluid pair. The driving force for the vapour transfer in the case of ammonia-
142 water and water-LiBr solution is considered to be the concentration difference and the water
143 vapour partial pressure difference across the membrane, respectively.

144 Membrane contactors have been extensively investigated for the desorption process in
145 absorption refrigeration systems, as the process in the desorber resembles that of a membrane
146 distillation process. In recent years, research is being performed to analyze the use of
147 membrane contactors in the absorber and solution heat exchanger. The principle of operation
148 and the use of membrane contactors in the desorber of absorption refrigeration systems can
149 alter the configuration of the cycle. However, the use of membrane contactors in the absorber
150 and solution heat exchanger has no effect on the configuration of the cycle.

151 Asfand and Bourouis [7] have performed an extensive review on the application of
152 membrane contactors in absorption refrigeration systems. They have concluded from their
153 review that the use of membrane contactors in the absorber and desorber of an absorption
154 refrigeration system can not only enhance the heat and mass transfer performance of the

component, but can also allow for a reduction in the size of the component. Thus, introducing polymeric hydrophobic microporous membranes into the absorber design could provide one of the alternatives for achieving highly compact absorbers, as microporous membrane contactors can provide a high specific surface area. Chen et al. [8] performed numerical simulations to study and evaluate the performance of an innovative hybrid hollow fiber membrane absorber. They reported that, for the same absorption rates, the volume of a hollow fiber membrane absorber was only 31% of that of a plate heat exchanger falling film absorber, while the mass transfer interfacial area was 4.3 times of that of a plate heat exchanger falling film absorber. Schaal et al. [9] analytically and experimentally analysed a hollow fiber membrane module absorber and reported that the membrane based absorber had a higher mass transfer rate when compared to the plate absorber. They concluded that the size of the absorber could be reduced up to 10 times more than plate absorbers, by utilizing the micro-porous hollow fiber membrane module. However, in their design cooling was not integrated into the hollow fiber absorber module. Ali [10] performed an analytical analysis to design a compact plate-and-frame absorber possessing a hydrophobic microporous membrane contactor at the aqueous solution–water vapour interface. His results demonstrated that the aqueous solution channel thickness greatly influences the absorber size compactness. Ali and Schwerdt [11] investigated experimentally and analytically the characteristics of membrane used in plate-and-frame membrane absorbers. In their experimental study, a solution film thickness of 4 mm was used and a differential pressure of nearly three times the pressure available in a typical absorber was applied. However, the absorption rate was approximately half that of the conventional absorbers. In a conventional absorber, the solution thickness flowing over a tube bundle varies from 0.1 to 1.0 mm. Ali [10] observed that reducing the solution film thickness from 2.5 to 1.0 mm can result in about a 20% increase in the absorption rate. In addition, results reported by Yu et al. [12] showed that a 3-fold increase in

the absorption rate is achieved when the solution film thickness is reduced from 0.15 mm to 0.05 mm. Thus, the low absorption rates obtained in the Ali and Schwerdt [11] analysis could be due to the higher values of the solution film thickness. Also they did not observe a change in the absorption rate when the vapour pressure potential was increased. They ascribed this behaviour to the dominant mass transfer resistance of their membrane. However, recent studies [13, 14] suggest that vapour pressure potential has a direct effect on the vapour mass transfer flux across the membrane and that the mass transfer through the solution is the dominant resistance rather than the membrane mass transfer resistance. Isfahani et al. [13] experimentally investigated a membrane based absorber for the absorption of water vapour in the aqueous solution of LiBr and reported that the absorption rate was 2.5 times higher than that in falling film absorbers. Isfahani and Moghaddam [14] experimentally analysed absorption characteristics of water vapour into a thin LiBr solution constrained by superhydrophobic nanofibrous membrane structures. They studied the effect of water vapour pressure, cooling temperature, solution film thickness and solution mass flow rate on the absorption rate in a membrane based absorber. They achieved an absorption rate of 0.006 kg/m^2s with a solution film thickness of 0.1 mm and a velocity of 0.005 m/s. Bigham et al. [15] experimentally and numerically investigated the implementation of micro-scale features on the flow channel surface to induce vortices within the solution film. They reported that the mass transport mode in such a configuration could be changed from a diffusive to an advective mode. They obtained an increase in the absorption rate by a factor of 2.5 i.e. from 0.0016 kg/m^2s to 0.004 kg/m^2s for the flow channel surface with micro-scale features.

Experimental and analytical analyses have been carried out to investigate the performance of the membrane based absorbers, however, detailed behaviour of the heat and mass transfer mechanisms at local levels in the channels and the fluid dynamic behaviour need to be

investigated to better understand the phenomenon and the effect of flow parameters. The objective of this work is to perform a computational fluid dynamic analysis of heat and mass transfer in a membrane based absorber that will help in designing a compact and efficient absorber. Ali [10] developed a one dimensional model to investigate the performance of a plate-and-frame membrane absorber whereas, Yu et al. [12] used a CFD solver based on Lattice Boltzmann Method (LBM) and finite difference method for the concentration and temperature field. In this work, a commercial CFD solver ANSYS/FLUENT 14.0, which is based on Navier-Stokes equations that are solved using finite volume method, is used to simulate the mass transfer across the membrane and the heat transfer between the solution and coolant in the absorber. Navier-Stokes equations are capable of solving both unsteady (time-dependent) and steady-state equations whereas Lattice Boltzmann equations are inherently unsteady and are more attractive to solve transient simulation. As in this study a steady-state analysis is performed therefore CFD solver based on the Navier-Stokes equation was selected as a favourable option. A plate-and-frame absorber module incorporating membrane contactor at the solution-vapour interface is selected for simulation with water-LiBr as a working fluid pair. A parametric study is performed to investigate the effect on the absorption rate of the solution channel thickness, solution flow rate and coolant wall temperature. The solution pressure drop along the channel length which is an important parameter of concern in water-LiBr based absorbers, working under vacuum condition, is investigated in detail. The effect of solution channel thickness and solution mass flow rate on the solution pressure drop along the solution channel length is critically analysed which was not previously reported. Further, the fluid dynamics behaviour of the water-LiBr solution is investigated and the effect of thermophysical properties on the solution flow profile is discussed as well. In addition, a case study is selected to analyse the boundary layers at the

solution membrane interface and the local profiles of velocity, temperature and concentration of the working fluid in order to better understand heat and mass transfer phenomena.

2. Membrane Absorber Configuration

The structural unit of the absorber configuration with membrane contactor is shown in Figure 1. The configuration of the plate-and-frame absorber is set as such that the lattice cell consists of a metallic plate for heat transfer and a microporous hydrophobic membrane sheet for both the heat and mass transfer. The membrane contactor is placed at the aqueous solution–water vapour interface in the form of parallel sheet along metallic plates to create individual flow channels. The parallel assembly of the plates and membrane sheets minimizes the pressure drop through the absorber. Three thin channels of refrigerant, coolant and absorbent solution are formed. Each refrigerant channel serves two absorbent solution channels at each side. Similarly the coolant channel also serves two aqueous solution channels. The first and last cells of the module have half width coolant channels.

The absorbent solution and the coolant flow along the metallic plate in a counter flow direction during which only heat transfer takes place. Water vapour and absorbent solution are brought into contact with each other using the microporous membrane contactor. Only refrigerant vapours pass through the pores of the membrane. If the absorbent is a solution containing water, then a hydrophobic microporous membrane can be efficiently utilized to stop the solution from passing through the pores of the membrane. As the water vapour pressure is more than the partial pressure of the water vapour inside the solution, the water vapour is absorbed at the solution-vapour interface and then diffused into the solution film.

2.1 Membrane material characteristics

In this study, a flat sheet membrane contactor made of polypropylene material is used. The membrane material characteristics are tabulated in Table 1.

2.2 Thermophysical properties

In the ANSYS/FLUENT 14.0 code material database water-LiBr mixture is not available. Therefore, a mixture of H_2O-LiBr was created in the material panel of ANSYS/FLUENT 14.0 code and the thermophysical properties of the water-LiBr mixture were updated in the ANSYS/FLUENT 14.0 code database using user-defined functions. These thermophysical properties of the aqueous solution of lithium bromide are estimated as a function of solution concentration in lithium bromide and temperature. The density and viscosity of the aqueous solution of lithium bromide were calculated using the correlations developed by Lee et al. [16]. The thermal conductivity of the water-LiBr mixture was calculated using the correlation of DiGuilio et al. [17]. Specific heat capacity of the water-LiBr mixture was calculated using the correlation based on Mc Neely data [18]. The diffusion coefficient of water in the aqueous lithium bromide solution was calculated from the experimental data of Kashiwagi et al. [19] which was determined at constant temperature and different concentrations. However, at other temperature the diffusion coefficient was estimated using the equation given below.

$$\frac{D_1\mu_1}{T_1} = \frac{D_2\mu_2}{T_2} \qquad (1)$$

Where D is the diffusion coefficient, μ is the dynamic viscosity and T is the temperature. State 1 refers to the values calculated at 25 ^{o}C whereas sate 2 refers to the values calculated at any other temperature. A user-defined function was implemented in the ANSYS/FLUENT 14.0 code

to estimate the value of diffusion coefficient using the above procedure at different concentration and temperature of the solution.

3. Governing equations

In the present simulations of heat and mass transfer across the membrane and heat transfer between the solution and coolant in the absorber, the flow in each channel is a homogeneous single phase flow. As the species in the solution are well mixed, the relative velocity between the species is negligible. In the absence of relative motion the governing mass and momentum conservation equations for homogeneous flow are reduced to the single-phase form. Therefore, instead of a mixture model, single phase equations are used to perform the simulation with less computational effort. The continuity, momentum, energy and species transport equations are solved to perform steady-state heat and mass transfer analyses.

The general steady-state equation of continuity which is based on the conservation of mass is given by:

$$\nabla \cdot (\rho \vec{v}) = S_m \qquad (2)$$

Where ρ is the density and $\vec{v}$ is the velocity vector. S_m is the mass source term which is added to the continuity equation and it is the vapour mass that is absorbed into the solution at the solution-membrane interface. The mass source term S_m is added as a user-defined function at the solution-membrane interface to model the vapour mass transfer across the membrane. The driving force for the vapour mass transfer flux into the aqueous solution in a H_2O-LiBr absorber is the water vapour partial pressure difference. The mass transfer flux across the membrane is given by Martinez and Rodriguez-Maroto [20] as follows:

$$J = k_m (P_v - p_{ms}) \qquad (3)$$

Where P_v is the water vapour pressure and p_{ms} is the equilibrium water vapour partial pressure of the solution at the membrane pores entrance and is calculated at the solution-membrane interface as a function of the solution concentration and temperature using the vapour pressure correlation given by Uemura and Hasaba [21]. k_m is the membrane equivalent mass transfer coefficient which is expressed in Ali [10] as follows:

$$k_m = \frac{2}{3} \cdot \frac{\varepsilon}{\tau \cdot \delta_m} \cdot d_p \cdot \sqrt{\frac{2}{\pi} \cdot \frac{M_{H_2O}}{R \cdot T_m}} \qquad (4)$$

where, ε is the membrane porosity, τ is the tortuosity of the membrane, δ_m is the membrane thickness and d_p is the membrane pore mean diameter. M_{H_2O} is the molecular weight of water, R is the universal gas constant and T_m is the membrane mean temperature which is calculated as the average vapour and solution interface temperatures.

The steady-state momentum conservation equation has the following form:

$$\nabla \cdot (\rho \vec{v} \vec{v}) = -\nabla p + \nabla \cdot (\bar{\tau}) + \rho \vec{g} + \vec{F} \qquad (5)$$

where p is the static pressure, $\rho \vec{g}$ is the gravitational body force while $\vec{F}$ is the external body force which arises as a result of the interaction of the vapour mass added to the bulk solution. $\bar{\tau}$ is the stress tensor and is given by

$$\bar{\tau} = \mu \left[\left(\nabla \vec{v} + \nabla \vec{v}^T \right) - \frac{2}{3} \nabla \cdot \vec{v} I \right] \qquad (6)$$

where μ is the molecular viscosity and I is the unit tensor.

The steady-state energy equation has the following form:

311 $$\nabla \cdot \left(\vec{v}\left(\rho E + p\right)\right) = \nabla \cdot \left(k_{eff} \nabla T - \sum_j h_j \vec{J}_j + \left(\bar{\tau}_{eff} \cdot \vec{v}\right)\right) + S_h \quad (7)$$

312 where T is the temperature in K, k_{eff} is the effective thermal conductivity, $\vec{J}_j$ is the diffusion
313 flux of the specie j, h_j is the enthalpy of specie j and the third term on the right hand side is the
314 energy transfer from viscous dissipation. E is given as:

315 $$E = h - \frac{p}{\rho} + \frac{v^2}{2} \quad (8)$$

316 where h is the sensible enthalpy and is defined for the incompressible flow as follows:

317 $$h = \sum_j Y_j h_j - \frac{p}{\rho} \quad (9)$$

318 S_h is the heat source term which is included to incorporate the heat of absorption in the solution
319 and is added to the energy equation using a user-defined function. The heat of absorption S_h is
320 calculated as:

321 $$S_h = h_v - h_s + h_{dil} \quad (10)$$

322 where h_v is the vapour enthalpy, h_s is the solution enthalpy and h_{dil} is the heat of dilution. h_v was
323 calculated using the correlation reported by Florides et al. [22], h_s was calculated using the
324 correlation reported by Kaita et al. [23], h_{dil} was calculated from the data of McNeely [18].

325 The steady-state species transport equation for the prediction of the local mass fraction of each
326 specie is given as:

327 $$\nabla \cdot \left(\rho \vec{v} Y_i\right) = -\nabla \cdot \vec{J}_i + S_i \quad (11)$$

where Y_i is the mass fraction of specie *i*, S_i is the specie source term which is added at the solution-membrane interface using a user-defined function and is equal to the mass of the water vapour transferred to the solution at the interface. $\vec{J}_i$ is the diffusion flux of specie *i*, which is given as:

$$\vec{J}_i = -\rho D_{H_2O-LiBr} \nabla Y_i \qquad (12)$$

where $D_{H_2O-LiBr}$ is the mass diffusion coefficient of water in an aqueous solution of lithium bromide.

4. Numerical simulation

Numerical simulations were performed to analyse the heat and mass transfer processes in a plate-and-frame membrane absorber. CFD commercial code ANSYS Fluent 14.0 was utilized for the numerical simulation which employs a finite volume approach to discretize the governing Navier-Stokes equations into a set of linear equations. The computational domain, boundary conditions and numerical schemes adopted in this study are illustrated in the following subsections.

4.1 Computational domain and boundary conditions

A two-dimensional model was developed to simulate the flow, heat and mass transfer phenomena in a single unit of the plate-and-frame membrane module. Figure 2(a) shows a 2D sectional view of a single unit of the plate-and-frame membrane absorber. To reduce the computational time and get a converged solution without flow instabilities, the vapour pressure and temperature of the vapour channel are assumed constant, as the vapour coming from the evaporator is at a constant pressure and the heat transfer across the membrane is very low

because of low thermal conductivity of the membrane material. Therefore, the vapour channel is not considered in the computational domain of the simulation. Hence, the mass of water vapour is added as a source term at the solution-membrane interface. Symmetric boundary conditions are considered on the left side of the coolant flow channel to reduce the computational efforts. The computational domain is shown in Figure 2(b). The heat transfer plate between the solution and coolant is considered as a wall boundary condition. Inlet boundary conditions in the solution and coolant flow channels are considered as velocity inlets, while outlet boundary conditions are specified as pressure outlets. The coolant temperature profile along the channel obtained from the initial converged steady-state simulation was used as a coolant wall temperature profile for the rest of the parametric analysis to minimize the computational time using only the solution channel. A wall temperature function was imposed at the heat transfer plate using a user-defined function to incorporate the linearized change in coolant temperature along the channel.

The spatial domain of the simplified model was discretized into meshes fine enough to produce mesh-independent results. The grids were created in Gambit software and imported into ANSYS Fluent 14.0. Different grid sizes were tested for the 0.5 mm solution channel and the 15 x 15000 cells mesh size, with a minimum edge size of 0.00002 was selected for the simulation analysis. Both the boundary layers on the coolant side and the membrane side comprised of 4 cells each with a growth factor of 1.2. The remaining cells in the middle of the solution channel were of the same size. Grid independence test showed that the maximum error in the absorption rate was less than 1 % when the grid size was reduced by a factor of 2.

4.2. Numerical model and discretization scheme

The governing equations of continuity, diffusion and energy are used to perform a numerical analysis of combined heat and mass transfer in a plate-and-frame membrane absorber. As the

solution flow Reynolds number is low, a laminar model is selected for the analysis. The calculations were performed by a combination of the SIMPLE (Semi-Implicit Method for Pressure Linked Equations) algorithm for pressure-velocity coupling and the first-order accurate implicit scheme for the linearized discretized equation in the segregated solver. A second-order upwind discretization scheme was used to compute advection terms. For the energy and specie transport equation, a second-order discretization scheme was used. In the present work, the numerical computation is considered to have converged when the scaled residuals of the different variables (continuity, momentum, species and energy equations) are lowered by tenth orders of magnitude and the steady state results are analysed.

5. Results and discussion

CFD simulations are capable of predicting the detailed behaviour of heat and mass transfer at local regions, thus, a clear pattern of the temperature and concentration gradients and velocity profiles are obtained. In the following subsections, the numerical model is validated with data from the open literature and a parametric analysis is performed to investigate the effects of solution channel thickness, solution mass flow rate and coolant wall temperature on the absorption process. Based on the parametric analysis results, a suitable geometry with optimal input operating conditions is selected for a detailed analysis of heat and mass transfer at local levels.

5.1. Validation

The CFD numerical model was validated by reproducing the results of the numerical analysis performed by Yu et al. [12] for a membrane based absorber in which the Lattice Bolzmann Method (LBM) was used to investigate the heat and mass transfer phenomena in a 20 mm long and 0.05 mm thick solution channel with an inlet solution velocity of 0.0182 m/s, and an

inlet solution concentration and temperature of 60 % and 55 ºC, respectively. The local absorption rate obtained using the CFD simulation is compared with the results reported by Yu et al. [12] for the corresponding case. The CFD results show good agreement with the literature data as shown in Figure 3. The mean absolute percent error was found to be 4.82 % with a standard deviation of 0.0322.

5.2. Parametric study

In this section, the results of the parametric study performed to investigate the effect of operational and geometric parameters on the absorption rate are discussed. Solution channel thickness, solution mass flow rate and coolant wall temperature were varied to investigate their impact on the absorption rate. The input data in the parametric study correspond to the operating conditions of a typical absorption refrigeration system. These operating conditions and geometric dimensions are listed in Table 2.

Figure 4 shows the results of the analysis carried out to investigate the effect of the solution film thickness on the absorption rate. Solution mass flow rate and other input variables were kept constant in all the cases except the solution channel thickness which was varied from 0.25 mm to 2 mm. Figure 4 (a) shows the local mass transfer flux along the channel obtained for different values of the channel thickness. It is observed that the absorption rate increases with a decrease in the solution channel thickness. It can be noted that a higher absorption rate is achieved at the inlet of the absorber due to the low mass fraction of water in the solution at the inlet and a lower solution interface temperature. A decreasing trend in the absorption rate is observed in the first quarter of the absorber while a steady absorption rate is achieved in the later part of the absorber. Initially a high mass transfer flux is observed as the solution concentration in LiBr is high, however, the absorption rate decreases sharply as concentration

and temperature boundary layers are developed consequently forming a resistance to the absorption of water vapours in the solution. A steady mass transfer occurs in the later part of the channel as the coolant wall linearly dissipates heat of absorption and allows the solution to cool down and maintain the absorption capacity of the solution. Figure 4 (b) shows the overall mass transfer flux obtained for different values of the solution channel thickness. It is observed that the overall absorption rate increased by a factor of 3 when the solution channel thickness was reduced from 2 mm to 0.5 mm. Increase in the absorption rate is more significant for lower values of the solution channel thickness as seen in Figure 4 (b). This is because a thinner solution channel leads to a higher solution flow Reynolds number and consequently thinner temperature and concentration boundary layers are formed which enhance the heat and mass transfer coefficients. In addition, the concentration and temperature gradients across the channel are less pronounced in the bulk solution for the thinner channel when compared to the thicker solution channel. Figure 5 (a) shows how the overall percent pressure drop along the channel increases when the solution channel thickness is reduced. In this study, the solution pressure at the absorber exit is set at 813.5 Pa which is the corresponding saturation pressure at a water vapour temperature of 4 ^{o}C. The overall percent pressure drop is calculated with reference to absorber inlet pressure. It can be seen that the overall percent pressure drop increases exponentially when the solution film thickness is reduced. A 50% decrease in the solution film thickness causes an increase in the accumulative pressure drop by a factor of approximately 7.5. Figure 5 (b) shows the accumulative pressure drop along the channel length for different values of the solution channel thickness. It is observed that the pressures drop linearly along the channel length for thinner solution channels. However, for thick solution channels the pressure drop in the first quarter is very small when compared to the later part of the channel. The absorption rate is significant in the first quarter of the solution channel up to 100 mm in length. However, the

absorption rate decreases and remains constant in the remaining part of the absorber. Thus, reducing the channel length can lead to a higher overall absorption rate and a low pressure drop.

Figure 6 shows the effect of the solution flow velocity on the absorption rate for a 0.5 mm solution channel thickness. Solution inlet velocity is increased from 0.00118 m/s to 0.00944 m/s while all other input parameters are kept constant in the simulation of each case. Figure 6 (a) shows the local mass transfer flux along the channel obtained for different solution inlet velocities. It can be seen that the absorption rate increases with an increase in the inlet velocity of the solution. Initially a high mass transfer flux is observed as the solution concentration is high, however, the absorption rate decreases sharply as concentration and temperature boundary layers are developed and resist the absorption of water vapours in the solution. A steady mass transfer occurs in the later part of the channel as the coolant wall linearly dissipates heat of absorption and allows the solution to cool down consequently increasing the absorption capacity of the solution. Figure 6 (b) shows the overall absorption rate obtained for different values of the solution velocity. It is observed that the increase in the overall absorption mass flux is more significant initially as the increase in the solution velocity brings fresh layers of solution near the membrane interface which increases the absorption capacity. However, further increasing the solution velocity decreases the solution residence time and minimizes the diffusion of the vapour across the solution causing a negative effect on the absorption mass flux. The absorption rate was increased by a factor of 2.5 when the solution inlet velocity was increased from 0.00118 m/s to 0.00472 m/s. The overall percent pressure drop along the channel for different flow velocities is shown in Figure 7 (a). The pressure drop increases by a factor of approximately 2.1 when the solution flow velocity is doubled. For example, increasing the solution flow velocity from 0.00236

m/s to 0.00472 m/s resulted in an increase in the pressure drop from 187 Pa to 391 Pa. However, it is observed that the overall percent pressure drop does not increase more sharply at higher velocities. It was observed that the accumulative pressure drop along the channel increases linearly with an increase in the solution flow velocity. Figure 7 (b) shows the accumulative pressure drop along the 0.5 mm solution channel at different solution inlet velocities. It can be noted that the pressure drop is more significant in the later part of the solution channel for low solution inlet velocities. However, at higher solution inlet velocities, the pressure drops linearly along the channel length. For the solution inlet velocity of 0.00236 m/s, the pressure drop in the first quarter of the channel is only about 2% whereas about 45% of the pressure drop is observed in the last quarter of the solution channel. Thus, it can be concluded that reducing the channel length can significantly minimize the pressure drop along the channel length.

It is important to note that although both solution flow velocity and solution film thickness can be independently varied in a plate-and-frame absorber, an optimum value of solution flow velocity and solution film thickness have to be selected to minimize the pressure drop which can significantly affect the performance of an absorber operating with water as a refrigerant under vacuum conditions.

Figure 8 shows the effect of the coolant wall temperature on the absorption rate for a 0.5 mm solution channel of 100 mm length. The coolant wall temperature was varied from 25 – 30 ºC to 35 – 40 ºC while all other input parameters were kept constant in the simulation of each case. Figure 8 (a) shows the local mass transfer flux along the channel obtained for different coolant wall temperatures. It can be seen that the absorption mass flux decreases when the coolant wall temperature is increased. This is because with an increase in the coolant wall temperature, the heat of absorption is not well dissipated and thus the solution temperature

491 increases and lowers the absorption capacity of the solution. Figure 8 (b) shows the overall
492 absorption rate for different coolant wall temperatures. It can be seen that the absorption rate
493 decreases linearly with an increase in the coolant wall temperature. The absorption rate
494 decreases by a factor of 5 when the coolant wall temperature is increased from 25 – 30 ºC to
495 35 – 40 ºC.

496 **5.3. Case Study**

497 Optimum values of the solution flow velocity and solution channel thickness were selected
498 for detailed analysis and comparison of heat and mass transfer at local levels. A solution
499 channel thickness of 0.5 mm and a solution flow velocity of 0.00472 m/s, yielding a high
500 absorption rate and low pressure drop along the solution channel, were selected for a detailed
501 analysis of the absorption process and comparison with the 2 mm solution channel. Figure 9
502 shows the contour of a velocity profile at the exit of the solution channel. It can be seen that a
503 laminar flow profile of the velocity distribution is obtained because of low solution flow rates
504 along the rectangular channel. Fully developed flow profile is obtained at the exit of the 2
505 mm and 0.5 mm solution channels as shown in Figures 9 (a) and 9 (b), respectively.
506 However, temperature and concentration gradients do slightly affect the flow profile because
507 of the change in the solution density which causes buoyancy forces. It can be observed from
508 Figure 9 (a) that the flow velocity near the solution-membrane interface (right side) along the
509 solution channel is lower compared to the solution velocity near the heat transfer wall (left
510 side). This is because of the effect of buoyancy forces which are observed at the solution-
511 membrane interface due to the change in density. The density of the solution near the
512 solution-membrane interface is lower than in the bulk, as the concentration of water in the
513 solution is higher near the solution-membrane interface due to the absorption of water vapour
514 and the temperature of the solution is higher at the solution-membrane interface due to the

heat of absorption. However, in Figure 9 (b) the velocity varies uniformly across the channel at the outlet. This is mainly because of the low temperature gradient across the 0.5 mm channel. Therefore, the variation in buoyancy forces is not significant across the channel. Soret and Dufour effects are negligible in this study as there is a small temperature gradient across the channel and no chemical reaction takes place.

In Figures 10 (a) and 10 (b), contours of temperature profiles at the inlet, exit and at the mid of the channel are shown for the 0.5 mm and 2 mm solution channels, respectively. Figure 10 depicts temperature values at local regions different to those in the bulk solution and a temperature gradient is observed across the width of the channel. It can be seen that the temperature near the solution-membrane interface (right side) is higher than the bulk solution temperature. This is because of the heat of absorption at the solution-membrane-interface. The temperature difference between the bulk solution and the solution-membrane interface is higher (up to 1.5 ^{o}C) near the inlet of the channel and then decreases downward to a steady value of 1 ^{o}C along the 0.5 mm solution channel. This is because of the higher absorption rate at the inlet which generates more heat at the solution-membrane interface and thus a higher temperature gradient is observed. However, in case of 2 mm channel the temperature difference between the bulk solution and the solution-membrane interface is higher and is about 5 ^{o}C. It is observed that initially the thermal boundary layer formed in the 2 mm channel is about 2 to 3 times thicker than the thermal boundary layer in the 0.5 mm channel. Due to the formation of the thermal boundary layer a resistance to heat and mass transfer is observed. Therefore, a temperature gradient exists across the solution channel which is about 4 ^{o}C higher in the case of the 2 mm channel than the 0.5 mm channel. This shows that in the 0.5 mm channel heat is well dissipated from the solution-membrane interface to the coolant side. Similarly, it can be observed from Figures 11 (a) and (b) that the water concentration in

539 the solution is higher at the solution-membrane interface (right side) due to absorption of
540 water vapour at the interface. The water molecules diffuse across the solution at a low rate
541 due to the low diffusivity which gives rise to a concentration gradient across the solution
542 channel. The concentration boundary layer developed at the solution-membrane interface also
543 plays an important role in limiting the mass transfer rate. The concentration boundary layer in
544 the 2 mm channel is significantly thicker than in the 0.5 mm channel. The effect of the
545 formation of the concentration and thermal boundary layers in the solution channels near the
546 solution-membrane interface is reflected as a low local absorption rate because the formation
547 of these boundary layers limits the absorption capacity of the solution. The LiBr
548 concentration at the solution-membrane interface is approximately 1.8% lower than in the
549 bulk solution in the 0.5 mm channel.

550 The bulk solution temperature and concentration, coolant wall temperature, and solution-
551 membrane interface temperature and concentration are graphically represented along the
552 channel length in Figure 12. It can be seen that the bulk solution temperature decreases from
553 35.5 ºC to 26.5 ºC as it flows downward along the channel because of the heat transfer to the
554 coolant which temperature is adjusted as a wall temperature and varies linearly from 25 ºC to
555 33 ºC in the counter flow direction. Similarly, the interface solution temperature drops from
556 38.0 to 27.4 ^{o}C. The mass fraction of LiBr in the bulk solution decreases along the channel
557 length due to the absorption of water vapour in the solution. It is observed that both the bulk
558 solution concentration and interface solution concentration decrease at the same rate
559 therefore, a transverse concentration gradient along the solution channel exists till the end of
560 the solution channel. As the concentration difference between the bulk solution and solution-
561 membrane interface also acts as a driving force for the mass transfer, water vapour absorption
562 is observed till the channel exit. It is worth to note that the mass fraction of water in the bulk

563 solution and at the solution-membrane interface increase along the channel length, however,
564 both the bulk solution temperature and the solution-membrane interface temperature decrease
565 along the channel length which in turn causes a decrease in the partial pressure of water
566 vapour in the solution and an increase in the absorption capacity.

567 Figure 13 shows a comparison of the bulk solution concentration along the 0.5 mm and 2 mm
568 solution channels. It is observed that reducing the solution channel thickness enhances the
569 mass transfer rate and as a result the exit bulk solution concentration achieved in case of a 2
570 mm solution channel can be achieved at a length of about 0.115 m in case of 0.5 mm solution
571 channel. Thus, decreasing the channel thickness from 2 mm to 0.5 mm and reducing the
572 absorber length from 400 mm to 100 mm can decrease the solution space requirement by a
573 factor of 16, whereas the absorber size can be reduced by a factor of about 5.5 keeping the
574 same thickness of 1.5 mm and 1 mm for the coolant and vapour channels, respectively.
575 Further, for smaller channel length a lower pressure drop will be observed. Thus, considering
576 a thinner channel with reduced length can both allow higher absorption rates and lower
577 pressure drops along the channel. Therefore, reducing the channel thickness and length can
578 allow for the design of highly compact membrane absorbers.

579 From the contours of the thermophysical properties shown in Figure 14 for the 0.5 mm
580 solution channel, it can be observed that the solution thermophysical properties vary at local
581 levels based on the local concentration and temperature. It can be seen that the density of the
582 solution near the solution-membrane interface (right side) is lower because of the higher mass
583 fraction of water at the interface and the higher temperature caused by the heat of absorption.
584 Similarly, the viscosity and thermal conductivity of the solution vary at local levels due to the
585 variation of the water mass fraction in the solution and temperature at local levels. The effects
586 of density and viscosity at local levels on the solution flow can be seen in the velocity profile

of the solution at the exit of the channel as shown in Figure 9 (a) in which the velocity near the solution-membrane interface is lower due to buoyancy forces caused by the low density of the solution. The low velocity at the interface inversely affects the mass transfer mechanism by developing thermal and concentration boundary layers at the solution-membrane interface thus limiting the absorption process. The higher thermal conductivity near the solution-membrane interface has a positive effect on heat transfer and can enhance heat transfer from the interface to the bulk solution.

5.4. Discussion

From the above results, it is clear that a plate-and-frame membrane based absorber employing water-LiBr as a working fluid mixture could be an interesting alternative for the design of compact absorbers with enhanced heat and mass transfer. In this study, for a 0.5 mm solution channel with a solution inlet velocity of 0.00472 m/s, an overall absorption rate of the order 0.001 kg/m^2.s was achieved whereas, Isfahani and Moghaddam [14] achieved an overall absorption rate of approximately 0.006 kg/m^2.s at a solution channel thickness and flow velocity of 0.1 mm and 0.005 m/s, respectively. Similarly, Yu et al. [12] achieved an overall absorption rate of above 0.009 kg/m^2.s when the solution channel thickness and solution flow velocity were considered of the order 0.05 mm and 0.15 m/s. It is clear that decreasing the solution channel thickness can significantly increase the absorption rate. However, it is worth to mention that the pressure drop increases exponentially with decrease in the solution channel thickness. As the absorber of an absorption refrigeration system employing water-LiBr operates under vacuum pressure therefore the high pressure drop in the solution channel could result in critical problems. Bigham et al. [15] achieved an overall absorption rate of 0.004 kg/m^2.s at a solution velocity of 0.05 m/s and a channel thickness of 0.5 mm with micro-scale features implemented on the flow channel surface, however, it is expected that

611 the pressure drop could be very high in such a design due to the micro-scale features.
612 Absorption rate in an absorber is also dependent on the operating conditions of the absorber
613 and flow parameters. A higher absorption rate can be achieved at a higher inlet concentration
614 of LiBr in the solution and a higher vapour pressure difference. Similarly, low solution and
615 coolant inlet temperature and high inlet velocity can also enhance the absorption rate. Yu et
616 al. [12], Isfahani and Moghaddam [14] and Bigham et al. [15] considered higher vapour
617 pressure and solution inlet concentration which resulted in a higher absorption rate. It can be
618 concluded from the above discussion that although in a plate-and-frame membrane based
619 absorber the solution flow velocity and solution thickness can be varied independently
620 however the increase in the flow velocity and decrease in the solution thickness should be in
621 a manner to achieve higher absorption rate with minimum pressure drop. Similarly,
622 appropriate operating conditions should be adopted to avoid the risk of crystallization. In
623 addition, the membrane contactor characteristics such as pore size, porosity, membrane
624 thickness and tortuosity can also significantly affect the absorption rate. In the above
625 mentioned studies from literature, a pore size in the range of 1 μm to 6 μm, membrane
626 thickness of 20 μm, membrane porosity of 60% and a tortuosity of 1 were considered.
627 Membrane with ideal tortuosity equal to 1 means that the membrane pores are assumed
628 straight however, in a microporous membrane, the membrane pores have a meandering path
629 which causes vapour pressure drop and lower the absorption rate due to higher flow
630 resistance. In this study, the membrane tortuosity was calculated using the equation given in
631 Table 1. Similarly decreasing the membrane contactor thickness and increasing the pore size
632 and porosity have a positive effect on the absorption rate however a nominal value must be
633 selected keeping in view the membrane material mechanical strength and liquid entry
634 pressure.

Conclusions

The absorber is one of the major components in absorption cooling systems and has a direct effect on the size and performance of this equipment. Introducing polymeric hydrophobic microporous membranes into the absorber design can be one of the alternatives for achieving highly compact absorbers with enhanced heat and mass transfer. In this study, CFD simulation is used to perform a detailed analysis of heat and mass transfer at local levels in the flow channels. The simulation results provide a deep insight of the heat and mass transfer in the membrane based absorber. The results of CFD simulation are useful and can play an important role in the design of membrane based absorbers that use water as a refrigerant. The effect of important parameters like solution film thickness, solution flow velocity and coolant temperature on the performance of membrane based absorbers is studied and it can be concluded that the solution flow velocity and solution film thickness are important parameters that can significantly affect the mass transfer rate across the membrane. The absorption rate was increased by a factor of 2.5 when the solution inlet velocity was increased from 0.00118 m/s to 0.00472 m/s. Moreover, it was observed that the absorption rate increased by a factor of 3 when the solution channel thickness was reduced from 2 mm to 0.5 mm. However, it was observed that the pressure drop increases exponentially with a decrease in the solution film thickness, while it increases linearly with an increase in the solution velocity. It is recommended that the solution channel thickness and the solution flow rate should be optimized to obtain a higher absorption rate across a membrane with a minimum pressure drop. Therefore to design a compact and efficient plate-and-frame membrane absorber, an optimum value of 0.5 mm for the solution film thickness is suggested and a solution velocity in the range 0.003 – 0.005 m/s is recommended. The local absorption rate decreases slightly along the length of the channel which affects the performance of the

absorber. In addition, the pressure drop down the channel length is more significant in thinner channels thus an absorber length of 100 – 200 mm is suggested for a plate and frame membrane absorber.

Acknowledgements

This study is part of an R&D project funded by the Spanish Ministry of Economy and Competitiveness (DPI2012-38841-C02-02). Faisal Asfand gratefully acknowledges the Rovira i Virgili University for granting the Martí-Franquès research fellowship 2012 (2012BPURV-50) to pursue a doctorate degree.

References

1. Amaris C, Bourouis M, Vallès M. Effect of advanced surfaces on the ammonia absorption process with $NH_3/LiNO_3$ in a tubular bubble absorber. International Journal of Heat and Mass Transfer. 2014; 72:544 – 52.

2. Amaris C, Bourouis M, Vallès M. Passive intensification of the ammonia absorption process with $NH_3/LiNO_3$ using carbon nanotubes and advanced surfaces in a tubular bubble absorber. Energy. 2014; 68:519 – 28.

3. Medrano M, Bourouis M, Coronas A. Absorption of water vapour in the falling film of water-lithium bromide inside a vertical tube at air-cooling thermal conditions. International Journal of Thermal Science. 2002; 41:891 – 8.

4. Jeong S, Garimella S. Falling-film and droplet mode heat and mass transfer in a horizontal tube LiBr/water absorber. International Journal of Heat and Mass Transfer. 2002; 45:1445 – 58.

5. Islam MR, Wijeysundera NE, Ho JC. Performance study of a falling-film absorber with a film-inverting configuration. International Journal of Refrigeration. 2003; 26:909 – 17.

6. Yoon JI, Kwon OK, Bansal PK, Moon CG, Lee HS. Heat and mass transfer characteristics of a small helical absorber. Applied Thermal Energy. 2006; 26:186 – 92.

7. Asfand F, Bourouis M. A Review of membrane contactors applied in absorption refrigeration systems. Renewable & Sustainable Energy Reviews. 2015; DOI:10.1016/j.rser.2015.01.054.

8. Chen J, Chang H, Chen S. Simulation study of a hybrid absorber–heat exchanger using hollow fiber membrane module for the ammonia–water absorption cycle. International Journal of Refrigeration. 2006; 29:1043–52.

9. Schaal F, Weimer T, Hasse H. Membrane contactors for absorption refrigeration. International Sorption Heat Pump Conference 2008, September 2008, Seoul, KOREA.

10. Ali AHH. Design of a compact absorber with a hydrophobic membrane contactor at the liquid–vapor interface for lithium bromide–water absorption chillers. Applied Energy. 2010; 87:1112–21.

11. Ali AHH, Schwerdt P. Characteristics of the membrane utilized in a compact absorber for lithium bromide–water absorption chillers. International Journal of Refrigeration. 2009; 32:1886–96.

12. Yu D, Chung J, Moghaddam S. Parametric study of water vapor absorption into a constrained thin film of lithium bromide solution. International Journal of Heat and Mass Transfer. 2012; 55:5687–95.

13. Isfahani RN, Sampath K, Moghaddam S. Nanofibrous membrane-based absorption refrigeration system. International Journal of Refrigeration. 2013; 36:2297–307.

718 14. Isfahani RN, Moghaddam S. Absorption characteristics of lithium bromide (LiBr)
719 solution constrained by superhydrophobic nanofibrous structures. International Journal of
720 Heat and Mass Transfer. 2013; 63:82–90.

721 15. Bigham S, Yu D, Chugh D, Moghaddam S. Moving beyond the limits of mass transport
722 in liquid absorbent microfilms through the implementation of surface-induced vortices.
723 Energy. 2014; 65:621–30.

724 16. Lee RJ, DiGuilio RM, Jeter SM, Teja AS. Properties of lithium bromide-water solutions
725 at high temperatures and concentrations - II Density and viscosity. ASHRAE
726 Transactions. 1990; Paper 3381. RP-527:709–14.

727 17. DiGuilio RM, Lee RJ, Jeter SM, Teja AS. Properties of lithium bromide-water solutions
728 at high temperatures and concentrations - I Thermal conductivity. ASHRAE Transactions.
729 1990; Paper 3380. RP-527:702–8.

730 18. McNeely NA. Thermodynamics properties of aqueous solutions of lithium bromide.
731 ASHRAE Transactions. 1979; 85: 413–34.

732 19. Kashiwagi T, Kurosaki Y, Nikai I. Heat and mass diffusions in the absorption of water
733 vapor by aqueous solution of lithium bromide. Transactions of the Japan Society of
734 Refrigerating and Air Conditioning Engineers. 2012; 1:89 – 98.

735 20. Martınez L, Rodrıguez-Maroto JM. On transport resistances in direct contact membrane
736 distillation. Journal of Membrane Sciences. 2007; 295:28–39.

737 21. Uemura T, Hasaba S. Studies on the lithium bromide-water absorption refrigeration
738 machine. Technology Reports of Kansai University. 1964; 6:31–55.

739 22. Florides GA, Kalogirou SA, Tassou SA, Wrobel LC. Design and construction of a LiBr–
740 water absorption machine. Energy Conversion and Management. 2003; 44:2483–508.

741 23. Kaita Y. Thermodynamic properties of lithium bromide–water solutions at high
742 temperatures. International Journal of Refrigeration. 2001; 24:374–90.

743 24. ANSYS FLUENT UDF Manual. ANSYS Inc. Release 14.0. November 2011.

744 25. ANSYS FLUENT Theory Guide. ANSYS Inc. Release 14.0. November 2011.

745

746

747

748

749

750

List of Figures

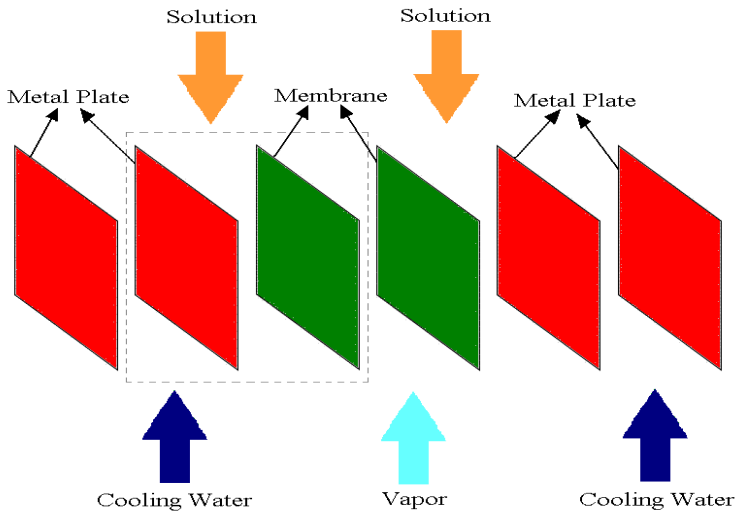

Figure 1: Plate-and-frame absorber configuration with membrane contactor

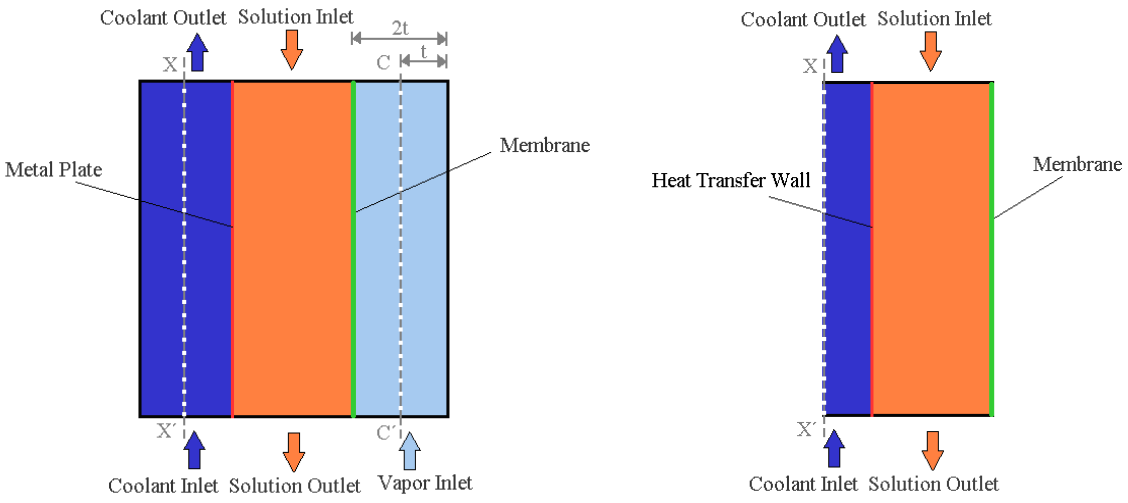

(a) Single unit of the plate-and-frame absorber (b) Computational domain of the plate-and-frame absorber

Figure 2: 2D sectional view of a single unit of plate-and-frame absorber

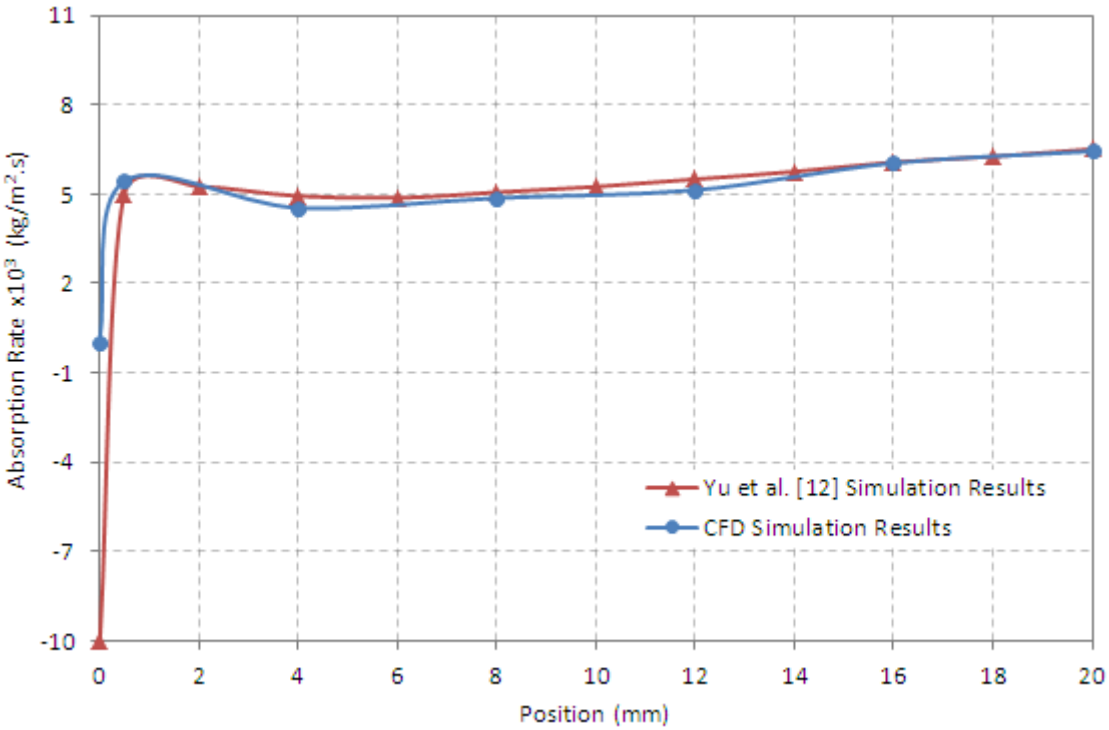

Figure 3: Comparison of the local absorption rate of the present work with data reported by Yu et al. [12]

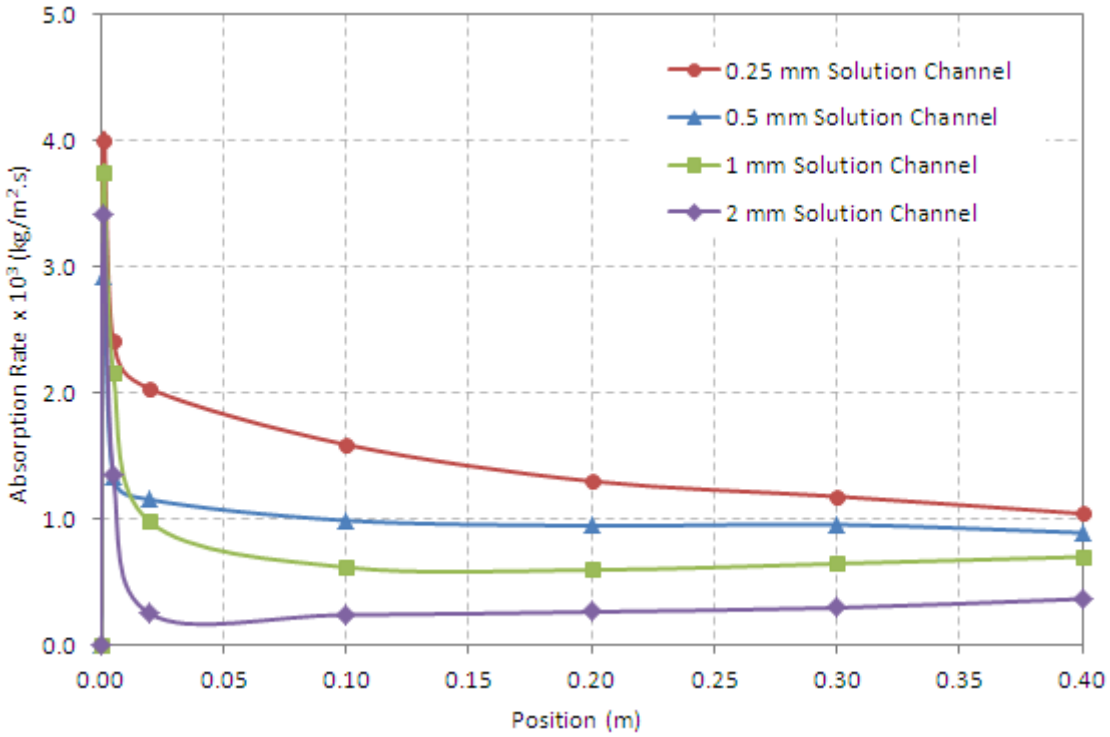

(a) Local mass transfer flux along the channel

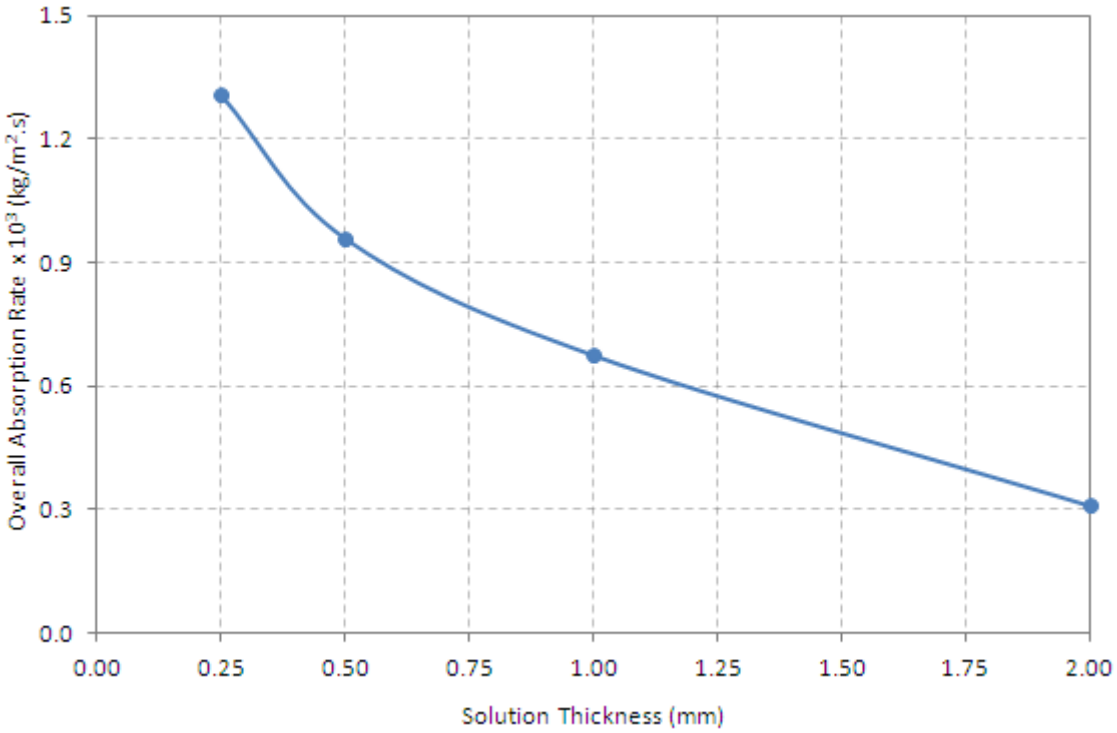

(b) Overall absorption rate

Figure 4: Effect of the solution channel thickness on the absorption rate along the channel

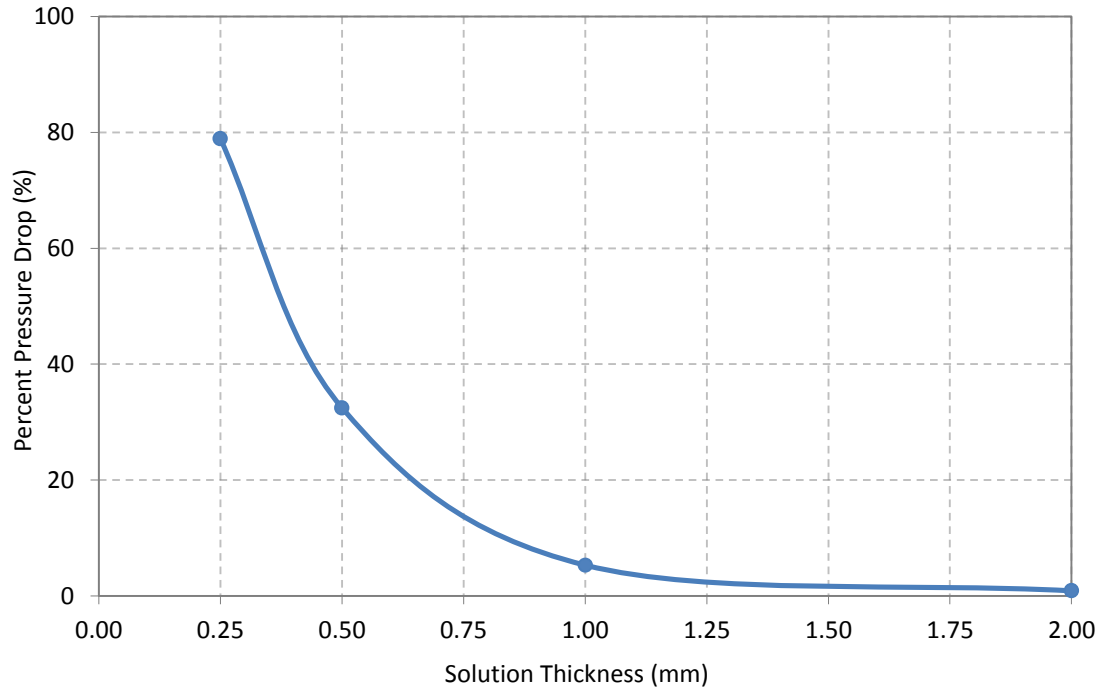

(a) Overall pressure drop vs solution channel thickness

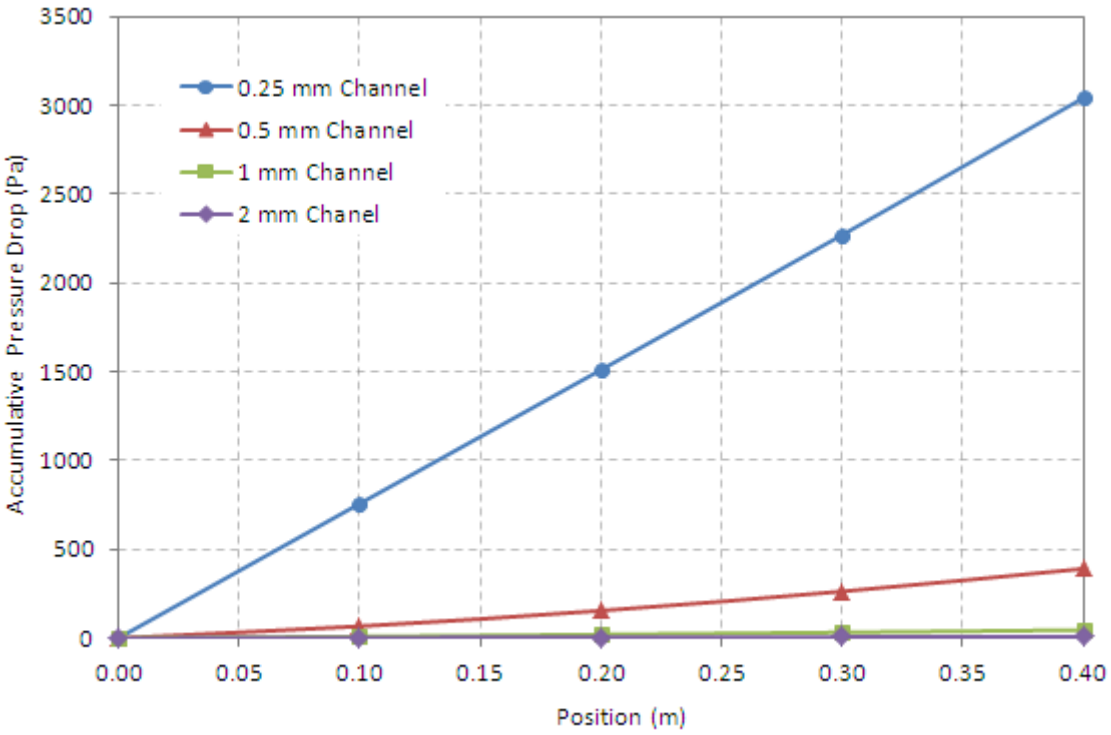

(b) Accumulative pressure drop along the solution channel

Figure 5: Effect of the solution channel thickness on the pressure drop

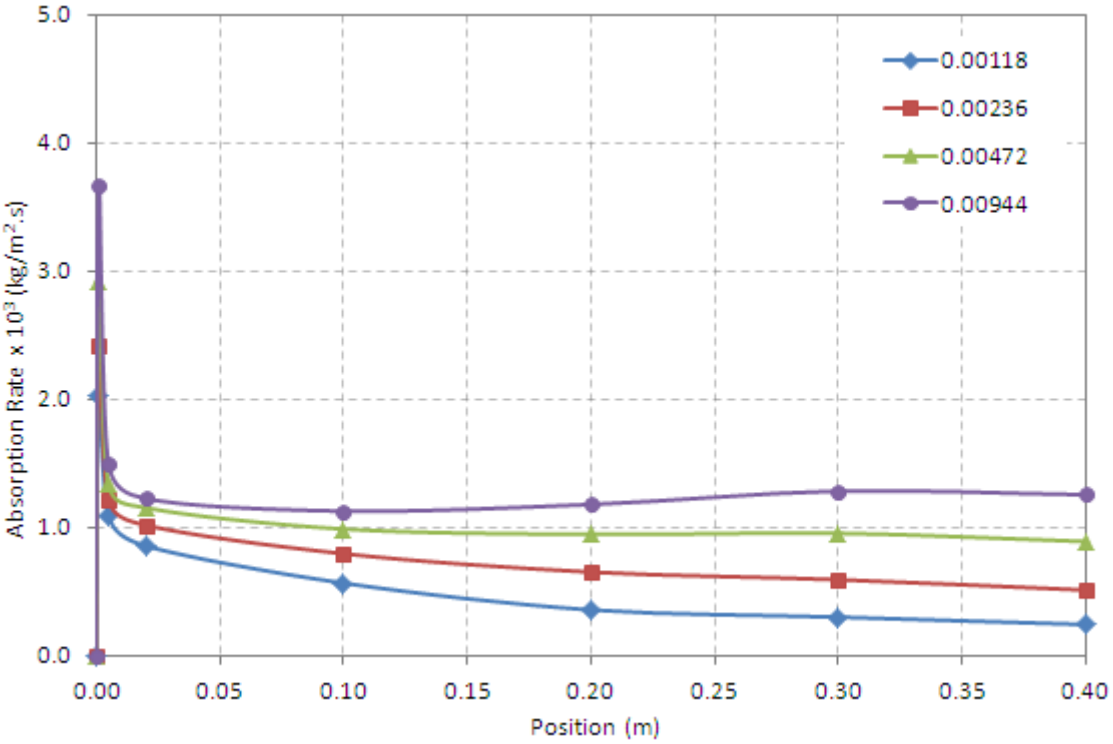

(a) Local mass transfer flux along the channel

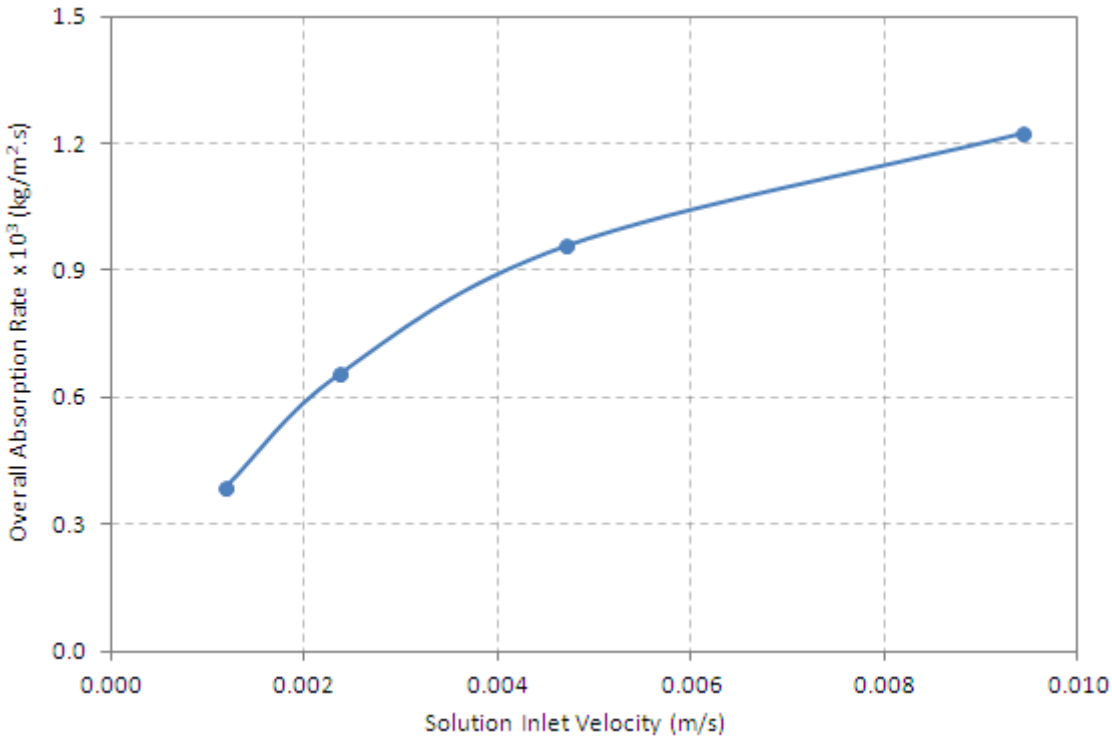

(b) Overall absorption rate

Figure 6: Effect of the solution flow velocity on the absorption rate along the channel

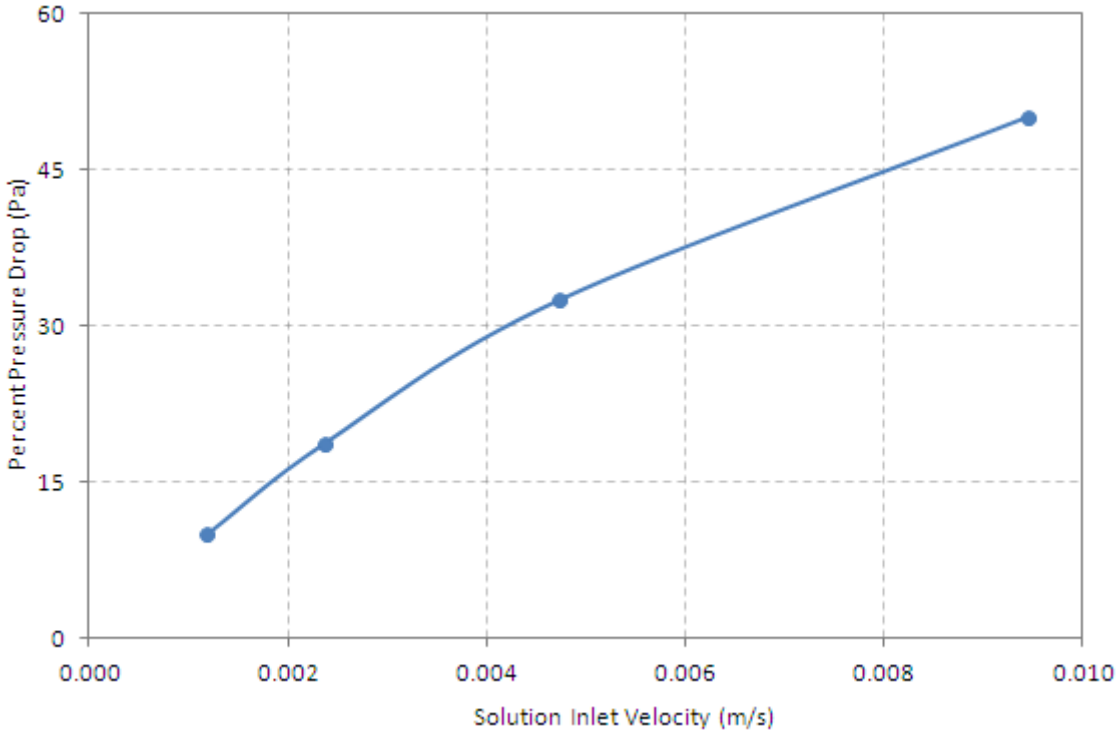

(a) Overall pressure drop vs solution inlet velocity

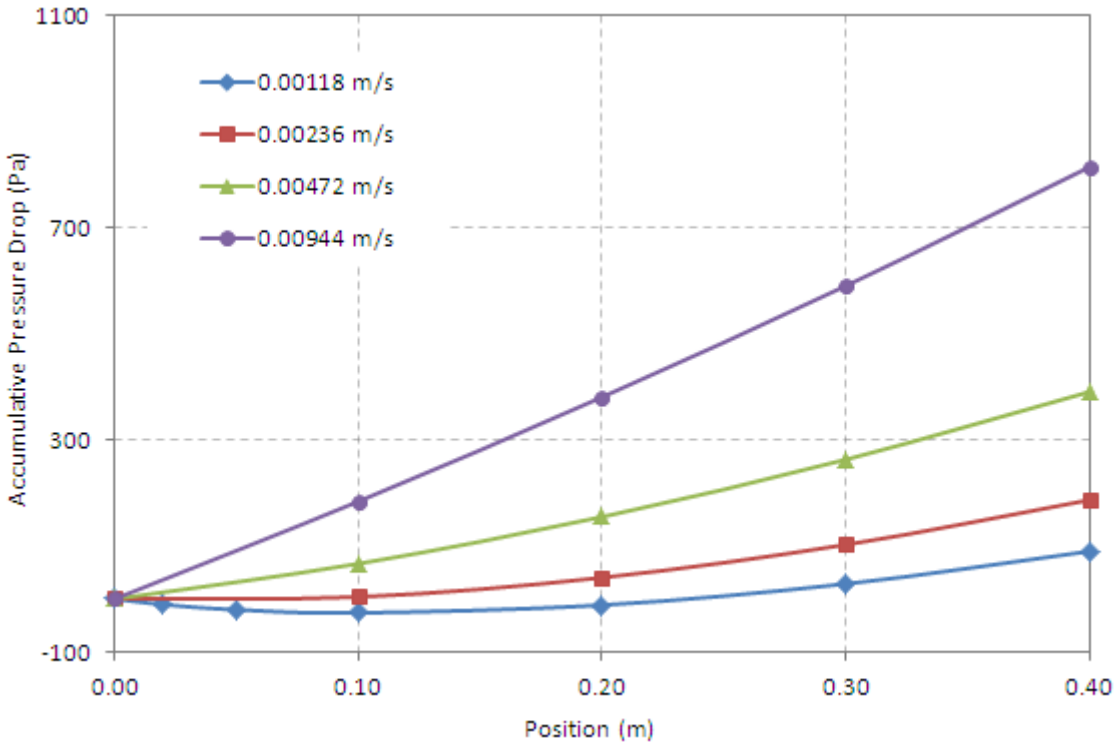

(b) Accumulative pressure drop along the solution channel

Figure 7: Effect of the solution flow velocity on the pressure drop

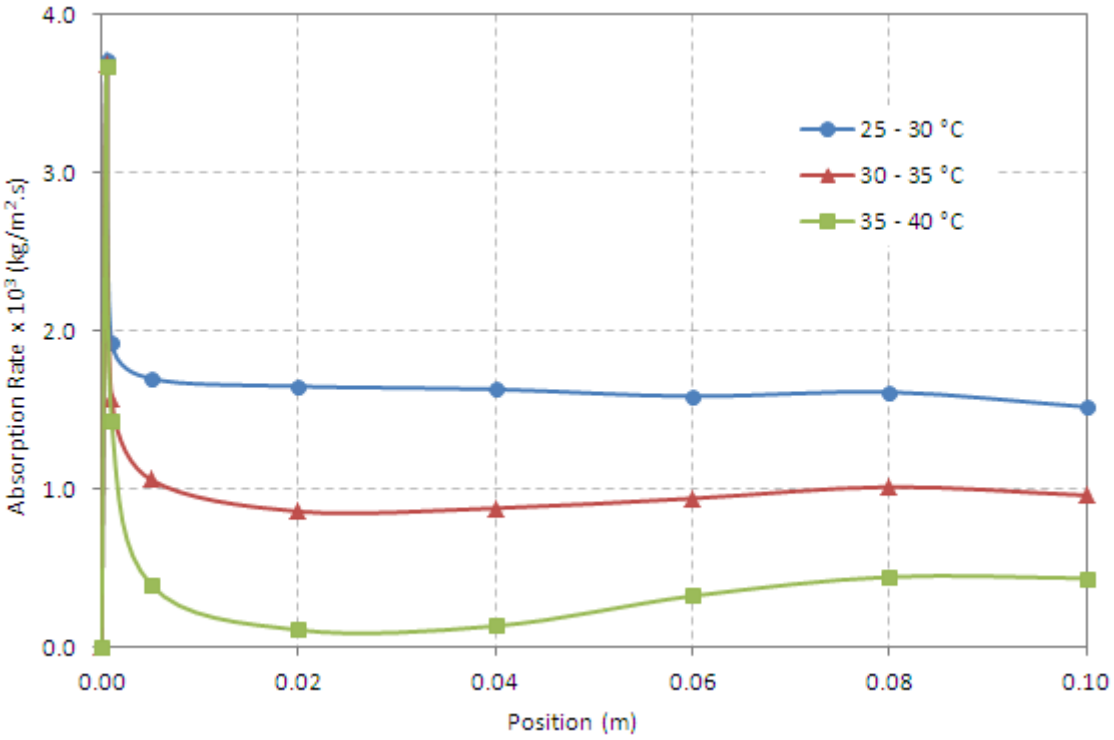

(a) Local absorption rate along the channel

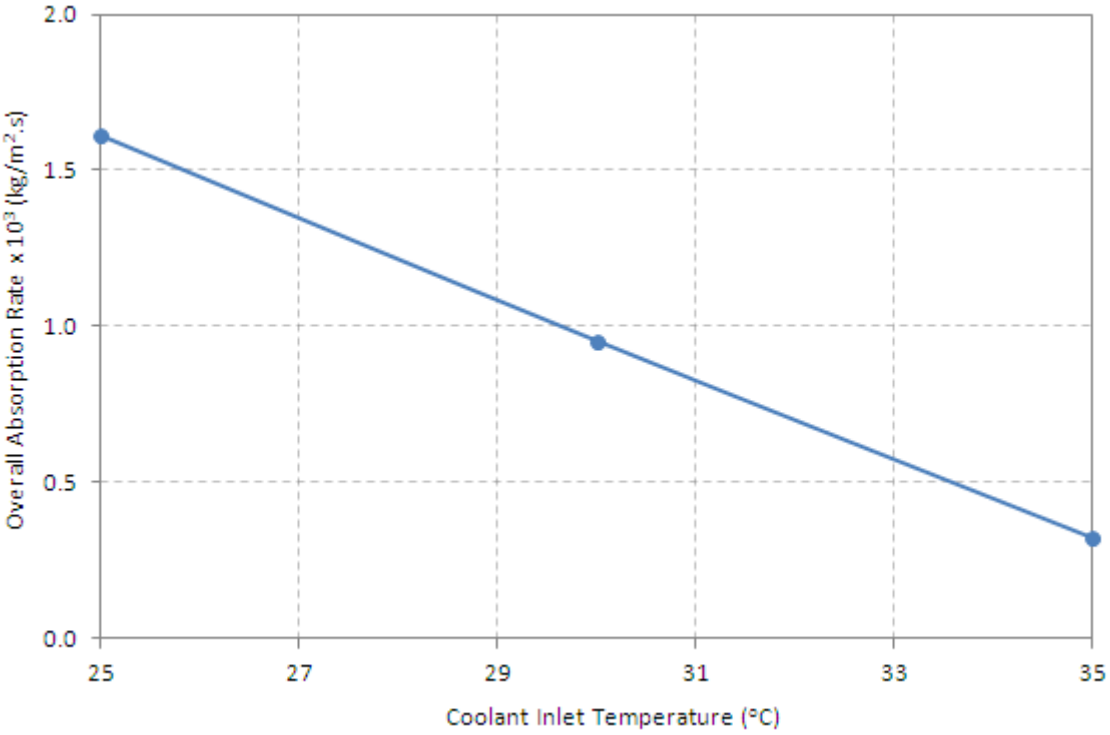

(b) Overall absorption rate

Figure 8: Effect of the coolant wall temperature on the absorption rate along the channel

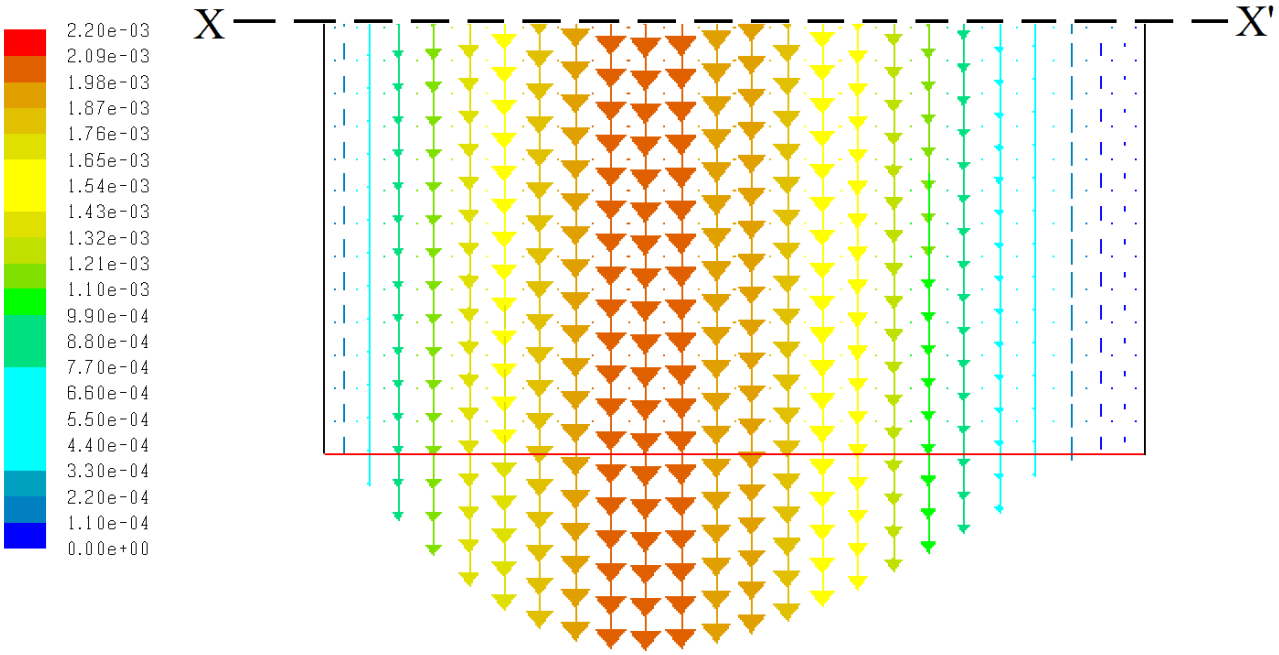

(a) 2 mm Channel

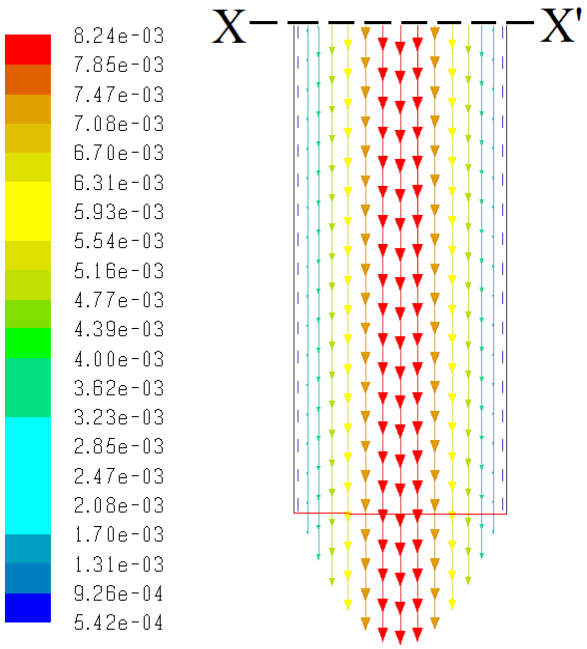

(b) 0.5 mm Channel

Figure 9: Contours of the velocity vectors (m/s) at the exit of the solution channel

822

823

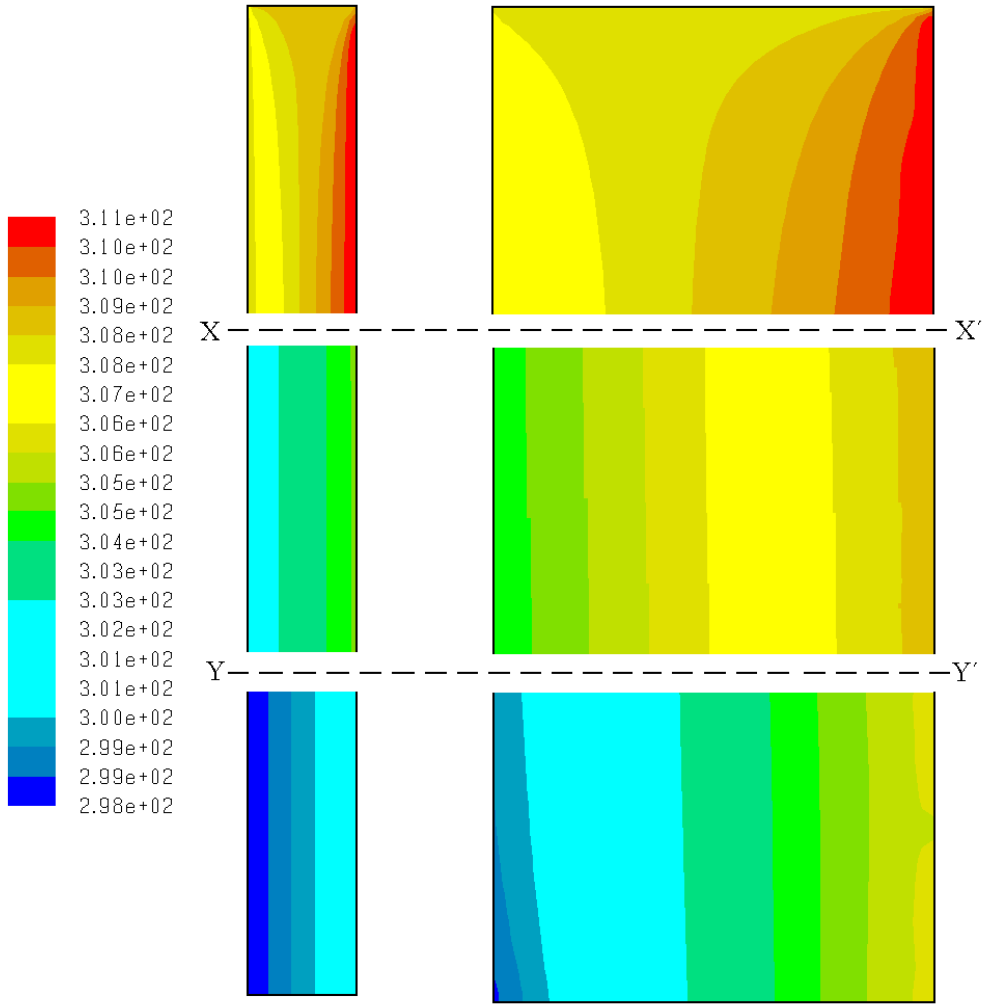

824

825 (a) 0.5 mm Channel (b) 2 mm Channel

826 Figure 10: Contours of the temperature (K) profiles along the solution channel

827

828

829

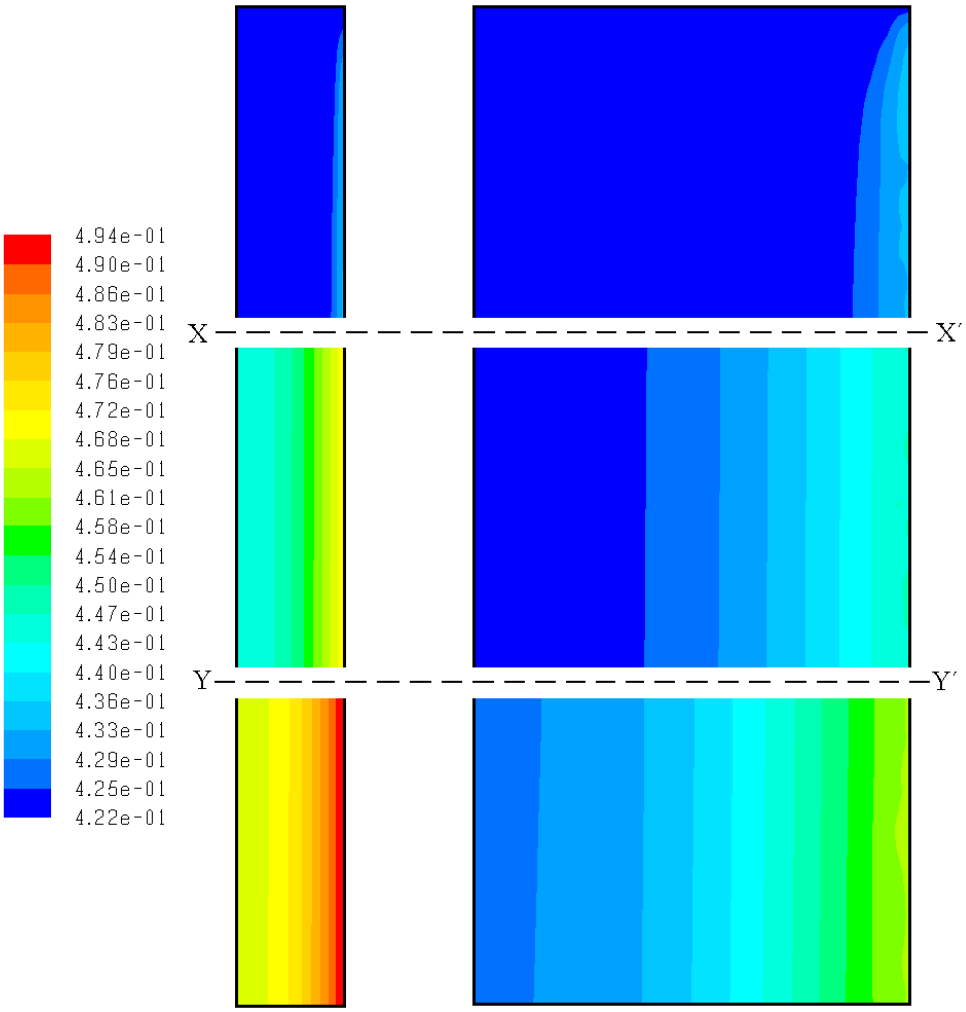

(a) 0.5 mm Channel (b) 2 mm Channel

Figure 11: Contours of the species concentration (H_2O mass fraction) profile along the solution channel

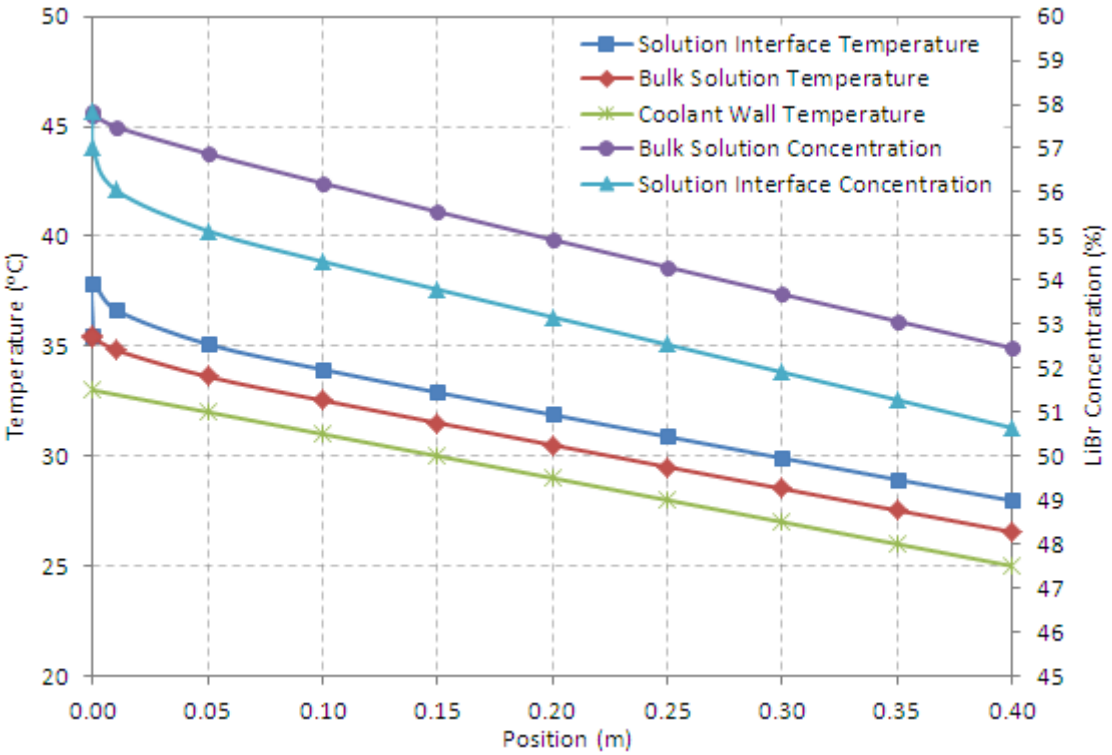

Figure 12: Temperature and solution concentration profiles along the solution channel

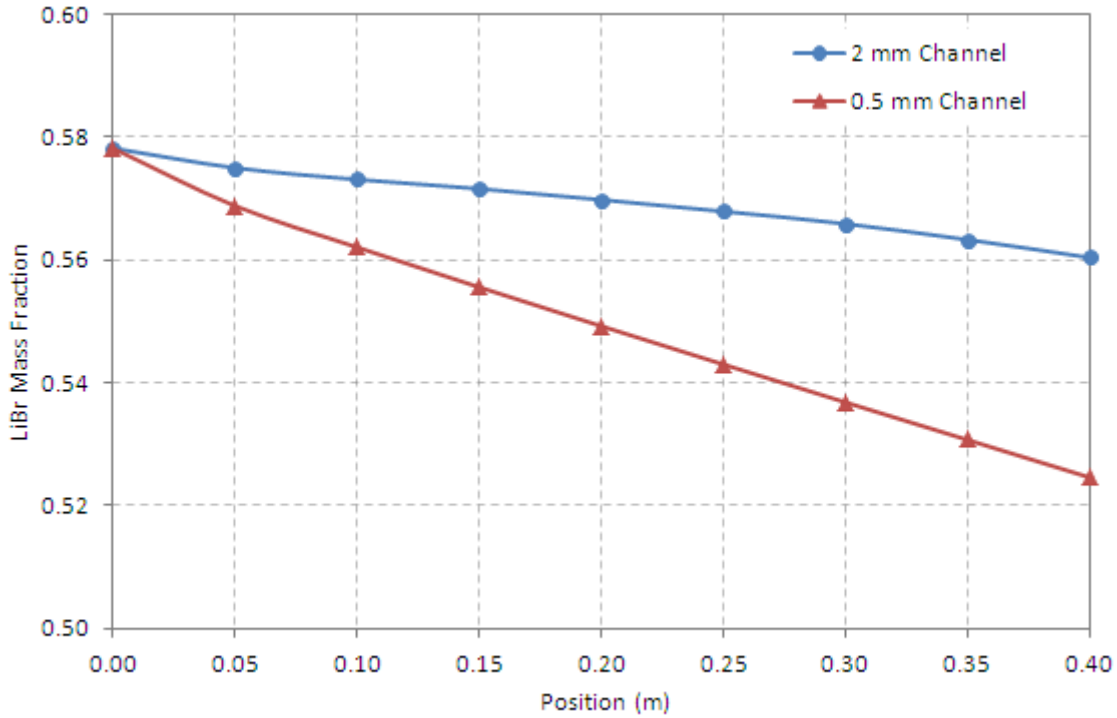

Figure 13: Concentration profiles in the bulk solution along the 0.5 mm and 2 mm solution channels

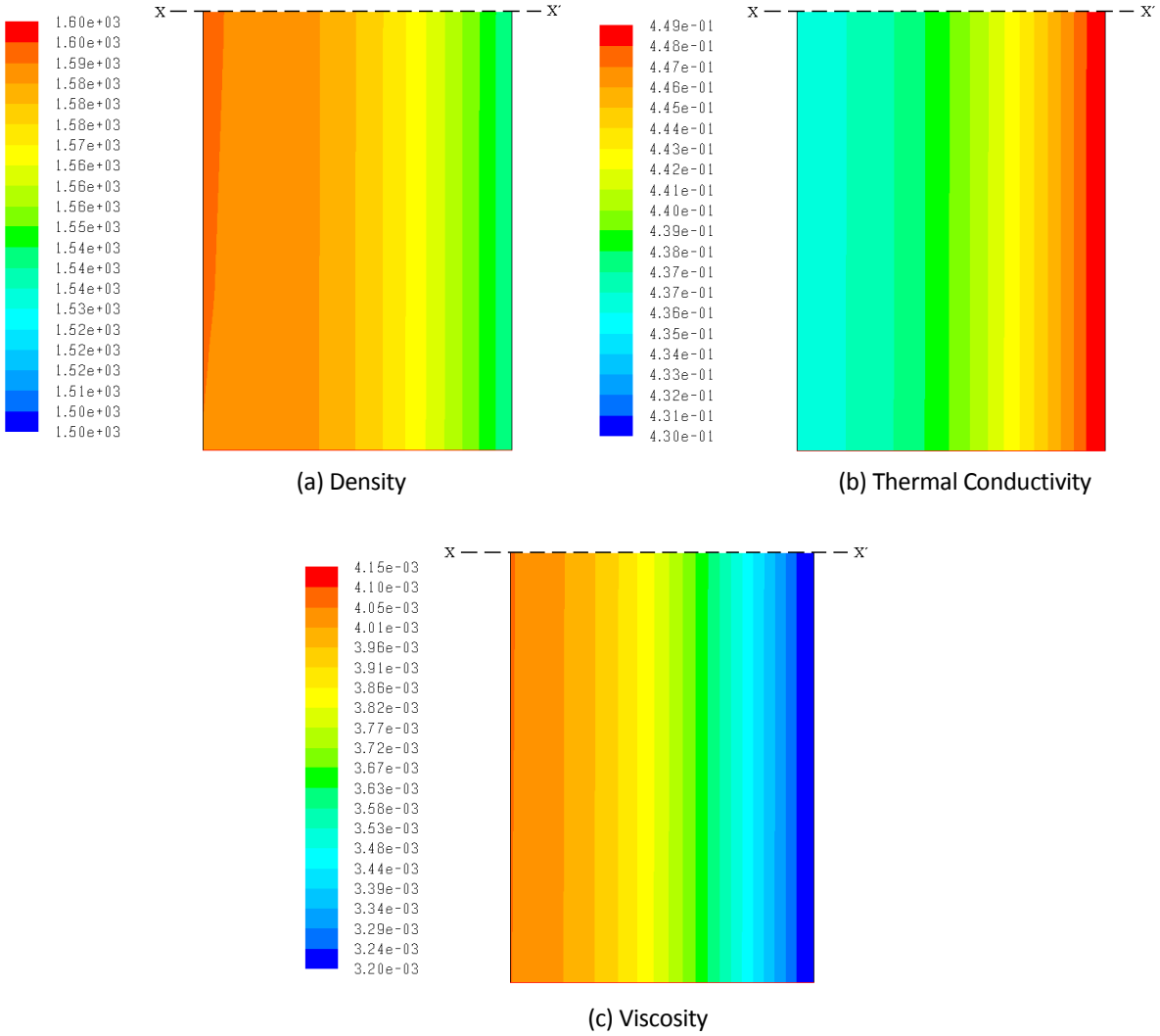

Figure 14: Thermophysical properties of the aqueous solution of LiBr corresponding to the solution concentration and temperature at the solution channel exit

List of Tables

883 Table 1: Membrane material characteristics

Thickness, δ_m (μm)	60
Porosity, ε (%)	75
Tortuosity, τ ($\tau = (2-\varepsilon)^2/\varepsilon$)	2.083
Mean pore diameter, d_p (μm)	0.45
Thermal conductivity, λ (W/m.K)	0.17

884

885 Table 2: Input data for the parametric study

Parameter	Base value	Range
Absorber pressure, Pa	813.5 Pa	NA
Inlet solution temperature, T_s	35.5 ºC	NA
Inlet solution concentration, X_s	57.82 %	NA
Solution velocity, $\vec{v}$	0.00472 m/s	0.00118 – 0.00944 m/s
Cooling wall temperature, T_c	25 – 33 ºC	25 – 43 ºC
Solution channel thickness, t	0.5 mm	0.25 – 2 mm
Solution channel length, L	400 mm	NA

886

887